I CLUSTER-DERIVED FTS CATALYSTS

Introduction

The Fischer-Tropsch synthesis (FTS) reaction is essentially a polymerization reaction as shown in reaction (1) and therefore can be analyzed using techniques developed to understand polymer chemistry.

$$CO + H_2 \longrightarrow [-CH_2-]_n + n\ H_2O \qquad (1)$$

The exact details of the mechanism are still the subject of considerable discussion.[1-4] However, it is generally agreed that FTS is a coordination catalyzed polymerization that proceeds by stepwise insertion of monomers into a metal-polymer bond.[5-9] Therefore, it resembles the Ziegler-Natta catalyzed polymerization of alkenes, which is the most frequently studied example of coordination catalyzed polymerization.[10-13] These two types of coordination catalyzed polymerization reactions are examples of the more general polymerization process called chain polymerization. Chain polymerizations proceed in three distinct steps: initiation, propagation, and termination. For coordination catalyzed polymerizations, termination is usually the elimination of the growing chain from the catalyst, and propagation is the insertion of the monomer unit into the metal-polymer bond, even though the exact nature of the monomer unit is not established for FTS. It is less clear if the analogy between Ziegler-Natta and FTS holds for the initiation step. For the Ziegler-Natta reaction, initiation is the generation of the active catalyst. For FTS, the initiation step is not well established but is generally thought to be reduction of CO to an alkyl (methyl) on the catalyst surface. Table I-1 compares these two coordination catalyzed polymerization reactions.

The last line of Table I-1 demonstrates the reason for the comparison: the product distribution is usually described by the

Table I-1

COMPARISON OF FTS AND ZIEGLER-NATTA REACTIONS

	Ziegler-Natta	Fischer-Tropsch
Reactant:	$RCH{=}CH_2$	$CO + H_2$
Product:	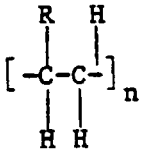	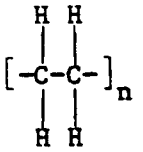
Initiation:	Generate active catalyst	Reduce CO to some active monomer
Propagation:	Monomer insertion	Monomer insertion
	$M{-}R + CH_2{=}CH_2 \longrightarrow M{-}CH_2{-}CH_2R$	$M{-}R + [CH_2] \longrightarrow MCH_2R$
		or
		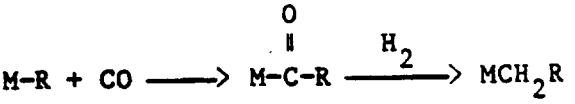
		or
		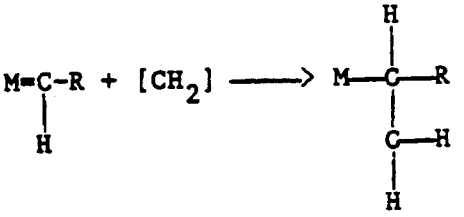
Termination:	β-Elimination (or others) $M{-}CH_2CH_2R \longrightarrow M{-}H + CH_2{=}CH{-}R$	β-Elimination (or others) $M{-}CH_2CH_2R \longrightarrow M{-}H + CH_2{=}CH{-}R$
Product distribution:	Poisson or Schultz-Flory	Schultz-Flory

Anderson-Schulz-Flory (ASF) distribution function for the FTS reaction and by the Poisson distribution function for the Ziegler-Natta reaction. However, the Ziegler-Natta reaction can give product distributions defined by either distribution function depending on the catalyst and polymerization conditions. A clear description of these two distribution functions is given in reference 9. Both are given in terms of mass distribution functions (m_p). The ASF distribution function is

$$m_p = \frac{(1 - \alpha)^2}{\alpha} p\alpha^p \qquad (2)$$

Where α is the probability of chain growth and p is the number of carbon atoms in the growing chain. The average degree of polymerization defined by the ASF distribution is

$$P_n = \frac{1}{1 - \alpha} \qquad (3)$$

The Poisson distribution is

$$m_p = \frac{e^{-\nu_\nu}(p-1)_p}{(p-1)!\ (\nu+1)} \qquad (4)$$

where ν is the average number of growth steps per molecule and is related to average degree of polymerization by

$$\nu = P_n - 1 \qquad (5)$$

The Poisson and ASF distributions are compared in Figure I-1 for the same average degree of polymerization.

As termination reactions become small relative to propagation reactions (i.e., $\alpha \longrightarrow 1$), a condition known as "living polymers," the product distribution is better described by the Poisson distribution.[12] Termination reactions have been virtually eliminated for a few low

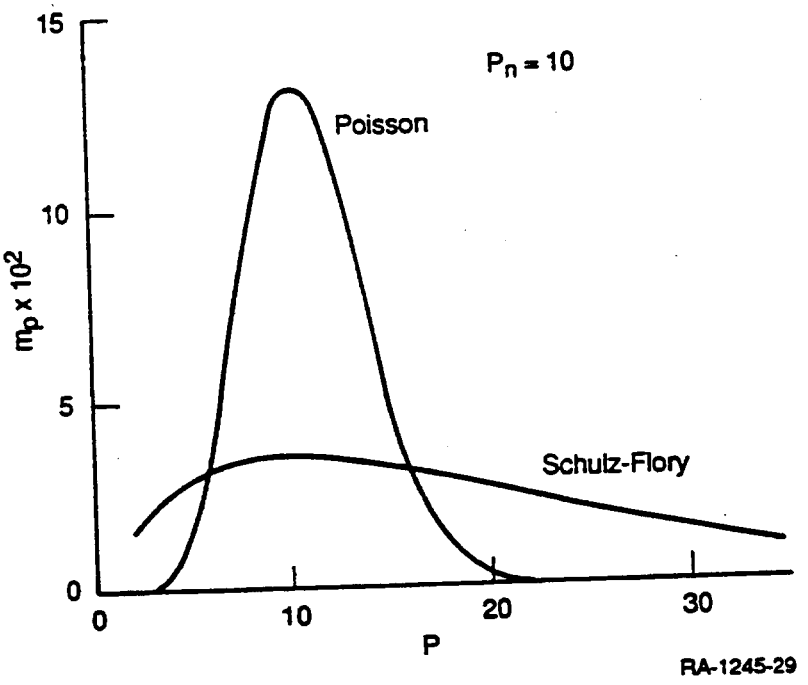

Figure I-1. Comparison of ASF and Poisson distribution for the same average degree of polymerization $P_n = 10$ (from reference 9).

temperature Ziegler-Natta polymerizations,[14] and very narrow product distributions (Poisson) have been observed experimentally for those systems.

However, if termination reactions are eliminated and all other factors held constant, the average number of polymerization steps increases. Extremely high molecular weight polymers would result, as in the case of high-density polyethylene. For Ziegler-Natta reactions, this result is desirable because polyethylene is wanted. However, it is not desirable for FTS reactions in which motor fuel range hydrocarbons are wanted. In Figure I-1, the maximum Poisson distribution and Schulz-Flory distribution is around 10 carbons for an average degree of polymerization (P_n) of 10. King has calculated the effect of P_n on the products of FTS using the ASF distribution function (Figure I-2), which shows that the maximum motor fuel yield is in the range of P_n = 5 to 8.[3] For Ziegler-Natta, P_n can be controlled by limiting the supply of monomer per active catalyst or by quenching at appropriate times after initiation. Neither action is appropriate for FTS operation as a continous process. King discussed alternative ways of limiting P_n that have appeared in the literature.[3] We conclude that to narrow the distribution of products from FTS we must increase the ratio of polymerization reactions to termination reactions (to get a Poisson distribution). However, to maximize the motor fuel yield, the number of polymerization reactions for each product must be limited to less than about 10.

Background

Strategy for Selection of Non-ASF FTS Catalysts

Figure I-3 shows the reaction products observed over a variety of catalysts at the indicated conditions.[15] Ruthenium catalysts have very high chain growth probabilities when operated at low temperatures and high pressures. Pichler et al. have reported the synthesis of polymethylene, whose properties are similar to those of low pressure polyethylene, over an activated ruthenium oxide catalyst at 132°C and

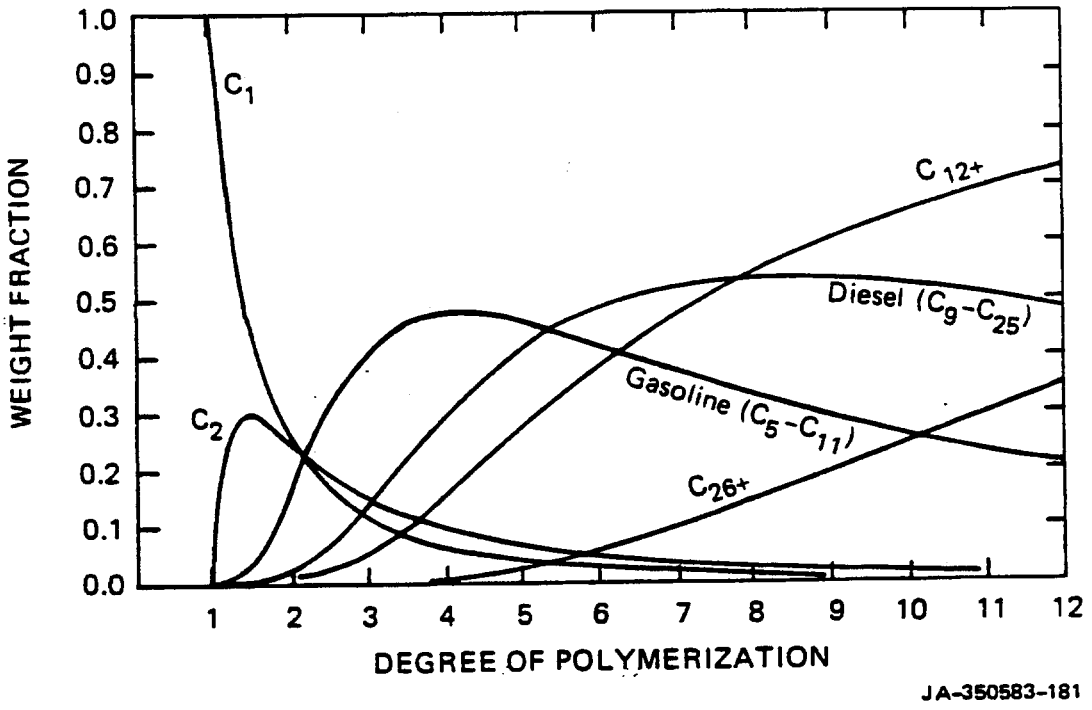

Figure I-2. Effect of average degree of polymerization (P_n) on the product mix for FTS with an ASF distribution (from reference 3).

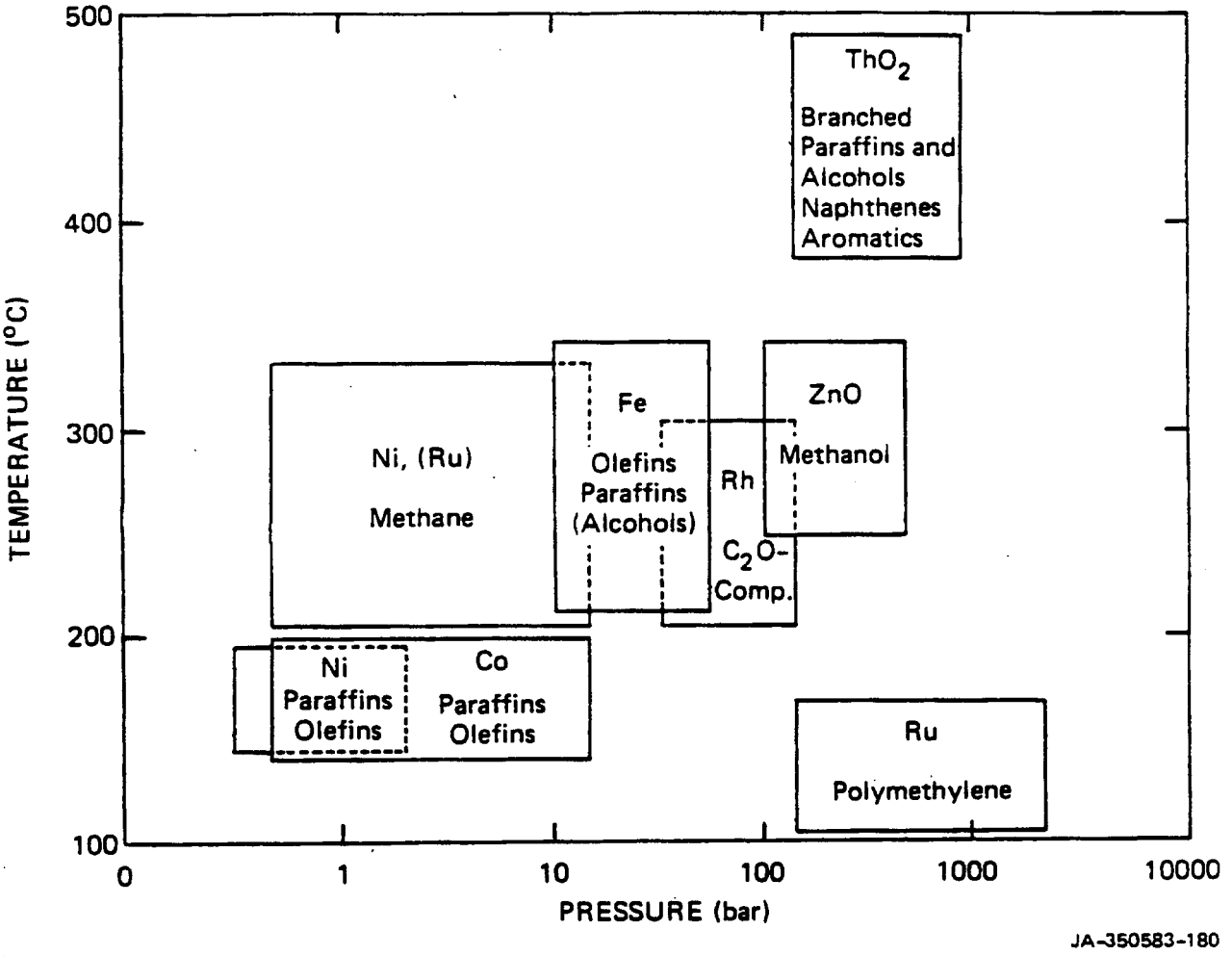

Figure I-3. Operating regimes for FTS catalysts (from reference 15).

1000 atm in a slurry reactor with water as the liquid phase and H_2/CO ratio of 2.[16] The molecular weight of the polymethylene product was reported to be over 100,000. In a similar experiment, Kolbel and coworkers slurried ruthenium metal in water and reacted with CO at 150°C and 200 atm to give parraffin waxes with molecular weight up to 7000.[17] This last reaction is an example of the Kolbel-Engelhardt reaction, which is closely related to FTS because the source of hydrogen is water. Despite the different source of hydrogen, the result is in good agreement with that of Pichler. Madon has also observed product distributions that deviate from ASF, as shown in Figure I-4, over a ruthenium catalyst at more reasonable process conditions of 241°C, 30 atm, and a heterogeneous reactor with space velocity of 193/h.[18] The extreme similarity of Figure I-4 implies that the product distribution observed by Madon is fit best by the Poisson distribution function. These three results strongly imply that over ruthenium catalysts at high pressures the chain termination reactions can be eliminated or significantly reduced so that the distribution approaches Poisson, as observed with Ziegler-Natta catalyzed polyolefin distributions.

Several other researchers have investigated the use of ruthenium as catalyst for FTS. In 1978, D. King compared supported and unsupported Ru and also compared supports.[19] He observed no significant deviations from an ASF distribution operating at 4 atm, 2/1 H_2/CO, and 175°-300°C. However, he reported that the reaction may be "mildly" structure sensitive. Bell and Kellner conducted a thorough kinetic study on alumina-supported Ru at 1-10 atm total pressure, H_2/CO ratio from 1/1 to 3/1, and 500-525 K temperature range.[20] Stowe reported that an Ru on alumina catalyst could be optimized to give a C_{2+} selectivity of 90% and a C_{6+} selectivity of 60%, of which 95% boiled at less than 500°F.[21] F. King and coworkers reported in 1985 a study of low weight loading Ru on alumina (0.3 %) at 210°C, 20-60 atm, and 2/1 H_2/CO ratio, which showed that at high pressures the selectivity to waxes was very high but apparently did not deviate from the ASF distribution.[22] Two reports have appeared on the effect of Ru particle size on FTS product distribution.[23,24] In both cases, hydrocarbon selectivities were greater for larger catalyst particles, although another group found the opposite result.[25]

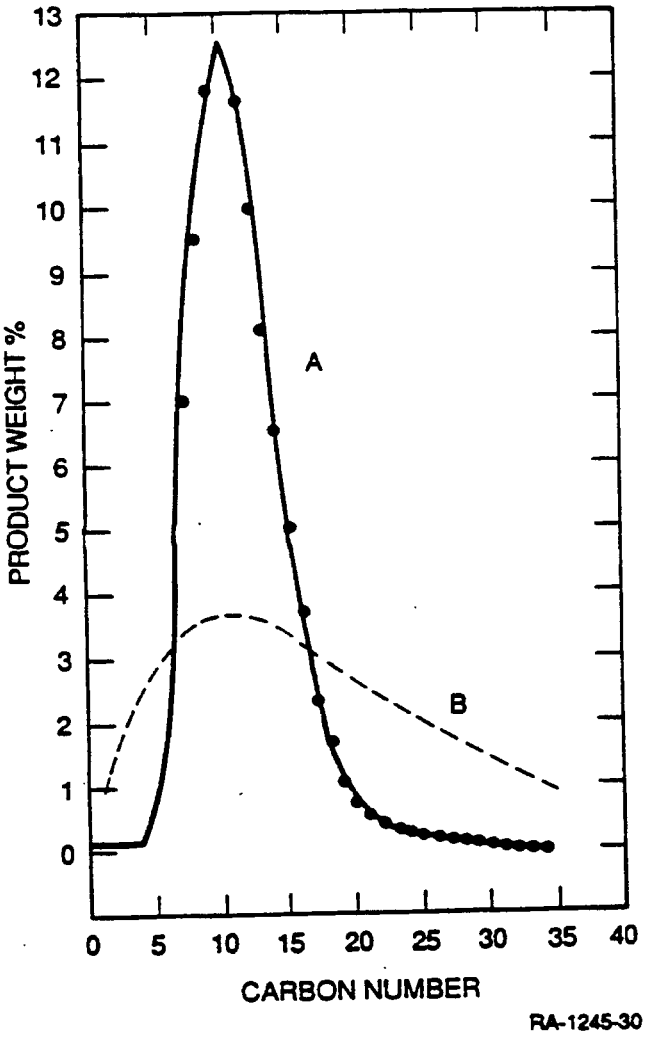

Figure I-4. Comparison of the product distribution (curve A) obtained by Madon over 1% Ru/Al_2O_3 at 241°C, 30 atm, and $H_2/CO = 2$ with the ASF theoretical distribution (curve B) (from reference 18).

Groups at the University of Tokyo and Tokyo Institute of Technology have studied the effect of promoters and particle size on supported Ru catalysts.[25-28] A group at Nagoya University has been studying the effect of nontraditional promoters such as rare earths and early transition metals.[29-33] They have found very high selectivities for C_5 through C_{15} hydrocarbons with rare earth and vanadium-promoted ruthenium catalysts. A second group at the University of Tokyo has been studying Ru-Pt bimetallic catalysts that selectively produce isoalkanes but with ASF product distribution.[34-36]

In 1979 Jacobs published a classical paper claiming that non-ASF distribution has been observed using Ru catalysts supported on zeolites.[37] He proposed that this effect was due to shape selectivity of the zeolite support. His results with Ru were rapidly confirmed for Fe[38] and Co[39] catalysts on zeolite supports. After further study, he changed the reason for non-ASF distributions in the FTS reaction from shape selectivity to an effect of the metal particle size.[40] He and Nijs developed an expanded ASF model that accounted for metal particle size and gave the observed non-ASF distributions by imposing a chain growth limitation related to the particle size.[41] Tkatchenko studied Fe, Ru, and Co on Y-zeolite and attributed selectivity for low-molecular-weight hydrocarbons to small metal particles.[42] Basset and coworkers reported non-ASF distributions on highly dispersed iron catalysts that disappeared as the catalysts aged because of sintering of the metal particles.[43] FTS studies over zeolite supported metals have continued in many laboratories in recent years with mixed results: some researchers have observed non-ASF distributions and others have not.[44-49] References 48 and 41 are most interesting. Lee and Ihm showed that the method of production of the metal particle on the zeolite affected the distribution; catalysts prepared from metal carbonyl precursors demonstrated selectivity.[48] Jacobs carefully studied an iron catalyst prepared from iron pentacarbonyl and Na-Y zeolite.[49] He was able to show that non-ASF distributions were observed only before the steady state, while the metal was being reduced. Once the metal was reduced, it agglomerated into larger particles that gave ASF distributions.

Jacobs and Van Wouwe critically reviewed the literature of non-ASF FTS reactions.[50] They concluded that it is very difficult to show that any reported deviations are real and result from mechanistic considerations rather than experimental artifacts. They suggested several explanations for the deviations and showed mathematically what the effect of each might be. The suggested effects include wax deposition, transient operation, sampling artifacts, secondary reactions, and mechanistic effects. The wax deposition theory is similar in concept to the encapsulation theory for deviations observed in Zeigler-Natta catalysis, which has been discounted.[51] However, for FTS, this effect was calculated by Dictor and Bell[52] with results that closely predict the experimental observations. The transient model has also been studied theoretically in detail.[53]

Since Jacobs's review, several articles have appeared reporting non-ASF distributions. Deviations over ruthenium catalysts were reported by several authors. Leith reports that for ruthenium supported on Y-zeolites, the hydrocarbon product distribution depends on particle size--larger particles give higher activity and higher hydrocarbons.[54] However, a reexamination of his data does not support his conclusion (Table I-2). His data indicate a very poor correlation of activity with particle size as measured by H_2 desorption. For any pair of catalysts using the same support, where differences in particle size were observed in the used catalysts, the activity was <u>greater</u> for smaller particles but the percent of C_{5+} was lower. Fukushima et al. studied Ru on SiO_2 by <u>in situ</u> FTIR techniques[55] and reached the same conclusion as Leith.[56]

Deviations from ASF have been reported for a number of other catalysts. Fujimoto et al.[56,57] report yields of 85% C_2-C_4 paraffins with less than 16% methane from a hybrid catalyst of a physical mixture of Pd/SiO_2 and Y-type zeolite. Fu and Bartholomew report that cobalt supported on alumina results in catalysts whose activity depends linearly on particle size[58] but have no significant deviations from ASF product distributions. Researchers at Mobil have reported the selective production of ethane over a dual-function catalyst composed of HZSM-5 zeolite containing Cr and Zn.[59] The selective formation of ethane has

Table I-2

LEITH'S DATA FOR Ru-Y CATALYZED FTS

Catalyst	Fresh Particle Size (nm)	Used Particle Size (nm)	Activity (mol s^{-1} g^{-1} Ru)	< $\%C_5$
RuMgY-I	4.3	4.9	160.2	23.4
RuNaY-I	4.9	4.6	72.9	19.2
$RuNH_4Y$-I	4.0	3.2	163.8	24.5
RuMgY-II	1.4	2.6	245.2	10.9
RuLaY-I	2.1	2.0	339.6	24.8
RuLaY-II	1.6	2.0	284.8	10.2
RuNaY-II	1.2	2.0	91.9	6.2
$RuNH_4Y$-II	2.3	1.7	247.6	15.4

also been reported by Iwasawa and Ito using a surface-confined mononuclear molybdenum catalyst on silica.[60] Their results are in distinct contrast to those of Somorjai et al., who studied CO hydrogenations over molybdenum single crystals and foils, which yielded primarily methane.[61]

Review of Synthesis Methods

A promising approach to preparing multifunctional catalysts was the unique process of surface confining, which permits the preparation of high-dispersion, high-activity catalysts through the reaction of organometallic compounds with support surfaces. Because the size, configuration, and metal composition of the homogeneous cluster (the catalyst precursor) can be defined a priori, these important parameters of the resulting catalysts are also well defined.

In the surface-confining process, functionalities on the metal cluster precursors are reacted with hydroxyl groups on the surface of the support to produce a surface-bound cluster. This technique has been used to prepare high-dispersion, high-activity catalysts for a wide variety of

reactions including oxidation, olefin metathesis, hydrogenation, reforming, hydrodenitrogenation, and FTS.

Surface-confined organometallic catalysts are prepared from two types of precursors: metal carbonyl clusters and metal hydrocarbyl complexes. Metal carbonyls can be reacted with supports as illustrated in reactions (6) and (7).

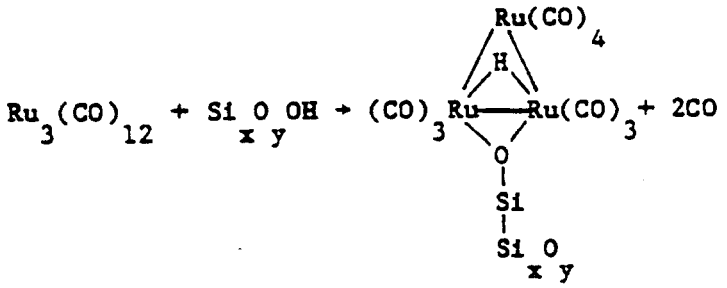

(6)

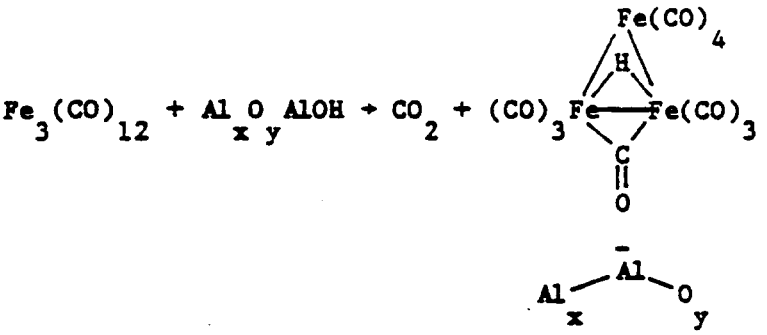

(7)

Metal hydrocarbyl complexes can be surface confined as shown in reaction (8).[62]

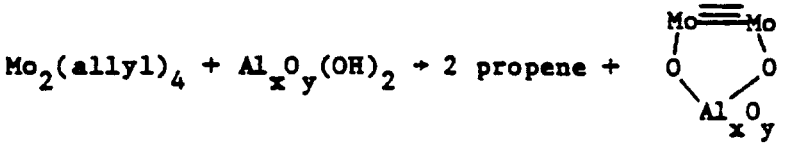

(8)

The preparation of surface-confined catalysts by reaction of organometallic compounds with supports is a rapidly expending area of research that has been the subject of several recent reviews. Researchers in North America and Western Europe have, for the most part, focused their attention on preparing surface-confined catalysts from the reactions of metal carbonyls with supports. The technique of preparing surface-confined catalysts by reacting metal hydrocarbyl complexes with supports has been extensively explored by Russian and Japanese researchers.

This method of catalyst preparation offers significant advantages over traditional impregnation techniques. For example, because the size, configuration, and exact metal composition (for intermetallics) of the organometallic cluster precursor can be designed before confinement, the initial surface-confined particle is totally defined. This feature is particularly useful for mixed-metal catalysts.

Selective control of particle size is a second major advantage of the use of surface-confined catalysts. Catalysts prepared by normal impregnation techniques contain a distribution of particle sizes only partially controllable through the conditions of catalyst preparation. Two problems result from this lack of control. First, the presence of larger clusters can result in a waste of metal in its interior. Second, a distribution of particle sizes can reduce catalyst selectivity. For structure-sensitive catalytic reactions, the particle size distribution can diminish the catalyst's potential selectivity for desired products.

Experimental Results

Synthesis

Surface-confined FTS catalysts were synthesized using a pendant hydrocarbyl functional group that reacts with hydroxyl groups on the surface of an appropriate support material. This work was divided into the following subtasks:

1. Synthesis of hydridocarbonyl ruthenium clusters.

2. Reaction of hydridocarbonyl clusters with alkyl aluminum to give alkyl aluminum carbonyl ruthenium clusters.

3. Reaction of alkyl aluminum carbonyl ruthenium clusters with the support.

4. Synthesis of alkyl complexes of ruthenium.

5. Reaction of alkyl complexes of ruthenium with the support.

Each subtask is described in detail below.

Subtask 1: Synthesis of Hydridocarbonyl Ruthenium Clusters. Three hydridocarbonyl ruthenium clusters, $H_2Ru_3(CO)_{11}$, $H_2Ru_4(CO)_{12}$, and $H_2Ru_6(CO)_{12}$, were synthesized using literature methods. Shore's method[63] was used to synthesize the hexaruthenium clusters.

$$Ru_3(CO)_{12} + Na[Ph_2(CO)] \xrightarrow[25^oC]{THF} 1/2\ Na_2[Ru_6(CO)_{18}] + Ph_2CO + 3\ CO \quad (9)$$

$$Na_2[Ru_6(CO)_{18}] + 2\ HCl \xrightarrow[25^oC]{THF} H_2Ru_6(CO)_{18} + 2\ NaCl \quad (10)$$

The infrared spectrum of $H_2Ru_6(CO)_{18}$ in dicloromethane solution exhibited (n_{CO}) bands at 2058(s), 2052(s), and 2003(w) cm^{-1} as expected. The ^1H NMR of $H_2Ru_6(CO)_{18}$ in CH_2Cl_2 shows a singlet at 8.80 ppm.

We achieved better yields and a purer product for the synthesis of $H_4Ru_4(CO)_{12}$ using our own technique, which involves the direct reaction of $Ru_3(CO)_{12}$ with H_2 in hexamethyldisilazane (HMDS) at elevated temperature.

$$4/3\ Ru_3(CO)_{12} + 2\ H_2 \xrightarrow[135^oC]{HMDS} H_4Ru_4(CO)_{12} + 4\ CO \quad (11)$$

The infrared spectrum of $H_4Ru_4(CO)_{12}$ in cyclohexane solution exhibited the expected CO stretching (n_{CO}) bands at 2081(s), 2067(vs), 2030(m), and 2024(s) cm^{-1}. The ^1H NMR spectrum of $H_4Ru_4(CO)_{12}$ in CH_2Cl_2 showed a singlet at -17.9 ppm.

For the synthesis of $H_2Ru_3(CO)_{11}$, we followed the method reported by Johnson et al.,[64] which entails the reaction of $Ru_3(CO)_{12}$ with sodium borohydride in tetrahydrofuran followed by treatment with acid.

$$Ru_3(CO)_{12} + Na[BH_4] \xrightarrow[25^oC]{THF} Na[Ru_3H(CO)_{11}] + 1/2\ B_2H_6 + CO \quad (12)$$

$$Na[Ru_3H(CO)_{11}] + HCl \xrightarrow[25^oC]{THF} H_2Ru_3(CO)_{11} + NaCl \quad (13)$$

The FTIR and NMR results for $H_2Ru_3(CO)_{11}$ indicated the presence of another unknown compound. We also tried Shore's method for the synthesis of this cluster and isolated a less pure compound. Attempts to purify this compound by recrystallization and by column chromatography were not successful. Since we were unable to prepare a pure sample in a reasonable time, we dropped this cluster from the approach.

Subtask 2: Reaction of Hydridocarbonyl Ruthenium Clusters with Alkyl Aluminum. A novel aspect of our approach to the synthesis of strongly bound ruthenium cluster catalysts was the intermediate synthesis of alkyl aluminum ruthenium carbonyl clusters just before reaction with the alumina support. Both the tetraruthenium and the hexaruthenium hydridocarbonyl complexes react readily with triethyl aluminum at room temperature. The reactions were carried out using procedures and techniques published for similar reactions. The reaction stoichiometries were determined by measuring the quantity of ethane produced. Gas chromatography indicated that only ethane was released; no trace of carbon monoxide was detected. Various amounts of ruthenium clusters (from 0.15 to 1.5 mmol) were used to react with excess triethyl aluminum to determine the reaction stoichiometries. For both the tetraruthenium cluster and the hexaruthenium cluster, the results are consistent with the production of one equivalent of ethane.

$$H_4Ru_4(CO)_{12} + Et_3Al \xrightarrow[25^oC]{THF} (Et_2Al)Ru_4(H)_3(CO)_{12} + EtH \quad (14)$$

$$H_2Ru_6(CO)_{18} + Et_3Al \xrightarrow[25^oC]{THF} (Et_2Al)Ru_6(H)(CO)_{18} + EtH \quad (15)$$

The reactions were allowed to continue overnight to assure complete reaction. In both cases, the color of the solution changed upon reaction, from yellow [$H_4Ru_4(CO)_{12}$] or purple [$H_2Ru_6(CO)_{18}$] to dark brown. Spectroscopic changes were also observed in the ^1H NMR and IR. These changes are summarized in Table I-3. The reaction of $H_4Ru_4(CO)_{12}$ with Et_3Al in benzene-d_6 was followed by ^1H NMR. New peaks appeared at 5.22 ppm (singlet), 4.10 ppm (AB doublet), and 2.01 ppm (triplet), which are tentatively assigned to the hydride, methylene protons, and methyl protons, respectively, of the $(Et_2Al)Ru_4(H)_3(CO)_{12}$ complex. The infrared spectrum of this new species in THF solution exhibited CO vibrational bands at 2037(m), 2030(m), 2016(s), 1998(s), and 1976(m) cm^{-1}.

Subtask 3: Reaction of Alkyl Aluminum Carbonyl Ruthenium Clusters with the Support. The two alkyl aluminum carbonyl ruthenium clusters, $(Et_2Al)Ru_4(H)_3(CO)_{12}$ and $(Et_2Al)Ru_6(H)(CO)_{18}$, each readily reacted with λ-alumina. The Bronsted acid site density of alumina (1 mmol/g) was determined by titration with ethyl lithium (described in Quarterly Report No. 3). Excess hydroxyl groups were available for reaction with the clusters if the metal loading was less than a few weight percent. The stoichiometries of the surface-confining reaction of the clusters with the supports were again determined by measuring the amount of ethane produced. Again, no carbon monoxide could be detected; only one equivalent of ethane was produced (with respect to the ruthenium cluster used).

$$(Et_2Al)Ru_4(H)_3(CO)_{12} + (AlO)\text{-}OH \quad [\text{support}] \xrightarrow[25^\circ C]{THF} (AlO)\text{=}O\text{-}Al(Et)Ru_4(H)_3(CO)_{12} + EtH \qquad (16)$$

$$(Et_2Al)Ru_6(H)(CO)_{18} + (AlO)\text{-}OH \xrightarrow[25^\circ C]{THF} (AlO)\text{-}O\text{-}Al(Et)Ru(H)(CO)_{18} + EtH \qquad (17)$$

Elemental analyses of the tetraruthenium cluster and hexaruthenium cluster catalysts on λ-alumina are presented in Table I-4.

Table I-3

FTIR AND NMR SPECTRA OF RUTHENIUM HYDRIDOCARBONYL CLUSTERS

Cluster	FTIR bands (cm^{-1})[a]	NMR peaks (ppm)[b]
$H_4Ru_4(CO)_{12}$	2081(s), 2067(s), 2024(s), 2030(m)	-17.9 (sgl)
$H_2Ru_6(CO)_{18}$	2058(s), 2052(s), 2003(w)	+8.8 (sgl)
$(C_2H_5)_2AlRu_4(H)_3(CO)_{12}$	2016(s), 1998(s), 2037(m), 2030(m), 1976(m)	5.22 (sgl) 4.10 (dbl) 2.01 (tpl)
$(C_2H_5)_2AlRu_6(H)(CO)_{18}$	2059(s), 2025(s), 1993(s), 2044(m), 1972(m), 1960(m), 1947(m)	5.78 (sgl)

[a](s), (m), (w) qualitatively refer to strong, moderate, and weak intensity, respectively, in the FTIR spectra.

[b](sgl), (dbl), (tpl), refer to singlet, AB doublet, and triplet peaks, respectively, in C_6D_6 solvent.

Table I-4

ELEMENTAL ANALYSIS OF RUTHENIUM CLUSTER CATALYSTS SUPPORTED ON λ-ALUMINA

Cluster	Ru	C	H
Ru_4	0.61	5.09	1.04
Ru_6	1.26	9.77	1.84

[a]Balance: Al, O, or Al_2O_3.

Subtask 4: Synthesis of Alkyl Complexes of Ruthenium. A monomeric ruthenium complex $[(allyl)_2Ru(CO)_2]$ was synthesized using literature procedures.[65,66] The procedure for synthesizing this compound is shown in the following equations:

$$Ru_3(CO)_{12} + 3\ (allyl)Br \longrightarrow 3\ (allyl)Ru(CO)_3Br + 3\ CO \quad (18)$$

$$(allyl)Ru(CO)_3Br + 2NaHg \longrightarrow Na^+[(allyl)Ru(CO)_3]^- + NaBr \quad (19)$$

$$Na^+[(allyl)Ru(CO)_3]^- + (allyl)Br \longrightarrow (allyl)_2Ru(CO)_2 + CO + NaBr \quad (20)$$

Allyl bromide reacts with ruthenium carbonyl in high yield to give $(allyl)Ru(CO)_3Br$ in high yield as reported.[66] The bromide can be reduced to the isolatable anion $[(allyl)Ru(CO)_3]^-$ using sodium amalgam. This anion reacts with allyl Grignard to give the desired product $[(allyl)_2Ru(CO)_2]$. A coproduct of the last reaction is carbon monoxide. We collected one equivalent of gas identified as CO by gas chromatography (GC). One reason we quantified the CO was to convince ourselves that we could quantify and correctly identify any CO given off in the subsequent reactions of the clusters with the supports.

Subtask 5: Reaction of Alkyl Complexes of Ruthenium with the Support. Monomeric ruthenium cluster catalysts were prepared on all three support materials, alumina, Na-Y zeolite, and molecular sieve zeolite, by reaction with $(allyl)_2Ru(CO)_2$ in THF solution at 25°C. No evolved gas product (e.g., propylene, propane, carbon monoxide) could be detected for reaction with λ-alumina. Therefore, the metal complex may have simply absorbed on the support.

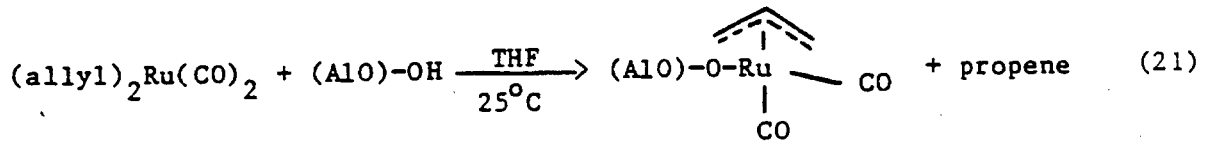

(21)

Elemental analyses of the monomeric Ru catalysts on all supports were performed by a commercial analytical laboratory (Galbraith Laboratory). The results showed ruthenium loadings ranging from 0.31 wt% for Ru/Na Y-zeolite to 0.37 wt% for Ru/λ-alumina.

Characterization

The supported catalysts were characterized by elemental analysis, FTIR, temperature-programmed desorption (TPD), and synthesis reaction stoichiometry. During the synthesis reaction, we measured loss of one ethylene per cluster and no loss of H_2 or CO. Therefore, the resulting supported catalysts were very similar in structure to the starting complexes. The FTIR confirms this. The diffuse reflectance FTIR of the alumina-supported hexameric cluster is shown in Figure I-5 as an example (the carbonyl stretching region is shown by the Kubelka-Munk expression). Three carbonyl stretching bands are observed at 2033, 2027, and 1970 cm^{-1}. These peaks are shifted by ~23 cm^{-1} from their position for the unsupported cluster. The peaks are approximately equal in intensity for the supported cluster, in contrast to the pattern of two strong and one weak observed in the spectra of the unsupported cluster.

The catalysts were analyzed by TPD in situ in the FTS reactor. The catalysts were tested from 300 to 573 K in a helium or hydrogen carrier gases at 0.167 K/s or 0.083 K/s. Figure I-6 shows the evolution of

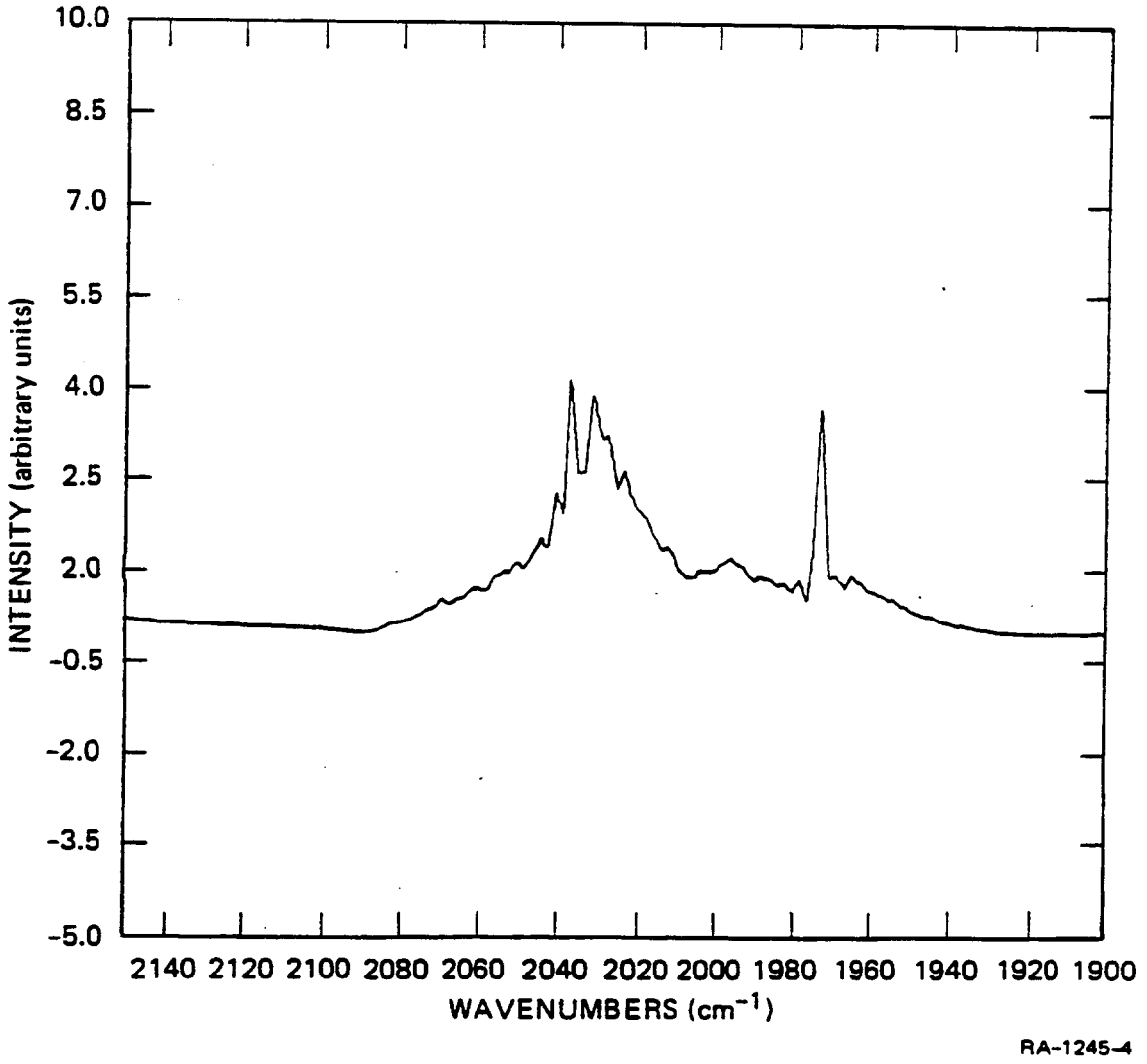

Figure I-5. Diffuse reflectance FTIR spectra for alumina-supported ruthenium hexameric carbonyl cluster catalyst before activation.

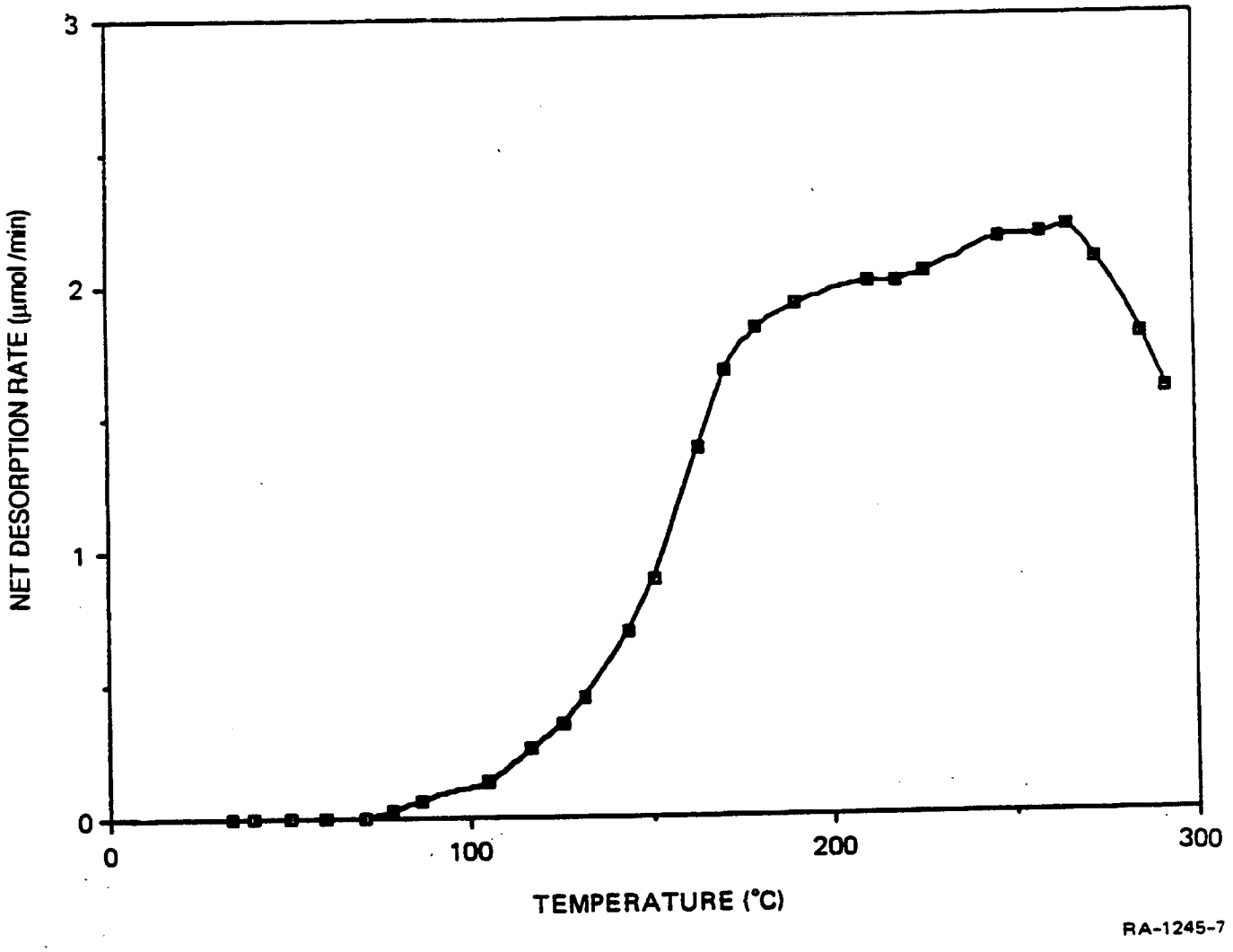

Figure I-6. Temperature-programmed desorption of Mass 28 for surface-confined ruthenium hexamer cluster catalyst.

Mass 28 starting at approximately 100°C at 0.167 K/s from the hexameric cluster catalyst in helium. This curve is indicative of continued reaction with the support upon heating. Most catalysts studied at 0.083 K/s in He showed onset of ethene evolution at approximately 433 K. At higher temperatures, C_1 and C_3 hydrocarbons were detected. TPD results are summarized in Table I-5. Temperature-programmed reaction (TPR) of all of these catalysts was also performed in 0.1 MPa hydrogen at 0.167 K/s. Methane was detected, and the reaction appeared to go to completion, indicating complete removal of the carbonyl ligands. Subsequent to activation, the catalyst was unloaded from the reactor and examined by FTIR to determine structural changes and sent for elemental analysis to

Table I-5

He TPD OF RUTHENIUM CLUSTER CATALYSTS
AT 5°/min UP TO 300°C

Catalyst	Temperature (°C)	Ethane or Ethylene (ppm)	Propane or Propylene (ppm)
Ru_5/5 Å mol, sieve	300°C	23.16	
Ru_6/Al_2O_3	250°C	44.31	
Ru_4/5 Å mol, sieve	250°C	56.61	
Ru_4/Na-Y zeolite	200°C	31.4	
Ru_4/Al_2O_3	200°C	47.0	
Ru/5 Å mol, sieve	260°C		35.9
Ru/LZY-52 zeolite	286°C		170.5
Ru/Al_2O_3	240°C		100.2

determine extent of changes in metal loading. Figure I-7 shows the FTIR of the hexameric cluster on alumina after He TPD to 300°C. Three broad bands are observed in the region from 2090 to 1910 cm^{-1}. The intensities of these absorptions are considerably smaller than observed for the

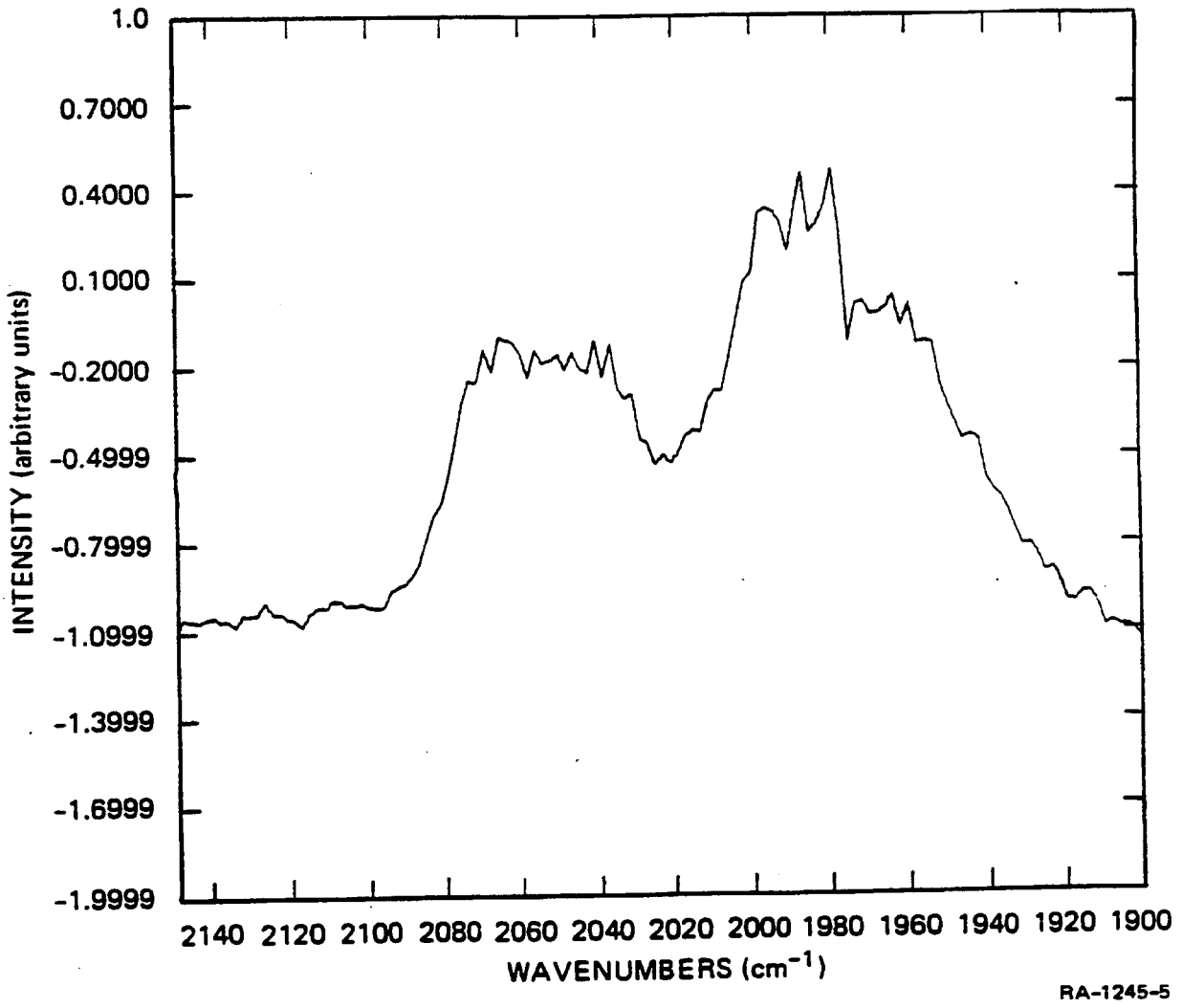

Figure I-7. Diffuse reflectance FTIR spectra for alumina-supported ruthenium hexameric carbonyl cluster catalyst after TPD.

sample before TPD, indicating loss of CO ligands. The loss of terminal CO stretching bands is most noticeable in the FTIR spectra, but new CO bridging bands appear. These changes in the FTIR spectra are indicative of major changes in structure caused by heating.

Catalysis

Fixed-Bed Reactor. A continuous flow quartz microreactor (Figure I-8) was used for FTS reaction studies. The catalyst sample (0.2 to 0.5 g) was placed on a fritted quartz disk located inside the reactor. Gaseous reactants fed to the reactor were purified: syngas, by passage through a molecular sieve trap cooled by dry-ice acetone; hydrogen, by diffusion through a Pd-Ag thimble; and helium, by passage through an oxygen trap. A quartz-sheathed chromel-alumel thermocouple situated in the catalyst bed continuously monitored the reactor temperature.

The FTS reaction was conducted with 0.1 MPa syngas. Syngas compositions of 2/1 and 1/1 (H_2/CO) were used. Reaction temperatures of 550 K and 573 K were used. A gas hourly space velocity of up to 12,000 was used to maintain approximately 10% conversion of carbon monoxide. The effluent from the reactor was continuously monitored by a quadrupole mass spectrometer and two gas chromatographs. The mass spectrometer and the automated two-column gas chromatograph (Carle) were used to follow the yield of methane, ethane, ethylene, carbon dioxide, and the overall CO conversion rate. Aliquots (0.1 mL) were withdrawn from the effluent of the reactor and injected into a second temperature-programmable gas chromatograph (Hewlett-Packard) with a wide-bore capillary column operating at 390 K and a flame ionization detector for analysis of higher hydrocarbons. The product distribution up through carbon number C_{12} could be measured with the dual GC system. The entire sampling system was wrapped with heating tape to prevent condensation of higher hydrocarbons.

The hydrocarbon reaction rate R is defined as the number of nanomoles of carbon monoxide converted into C_1 through C_{10} hydrocarbon per gram of catalyst per second. The selectivity S is defined as the

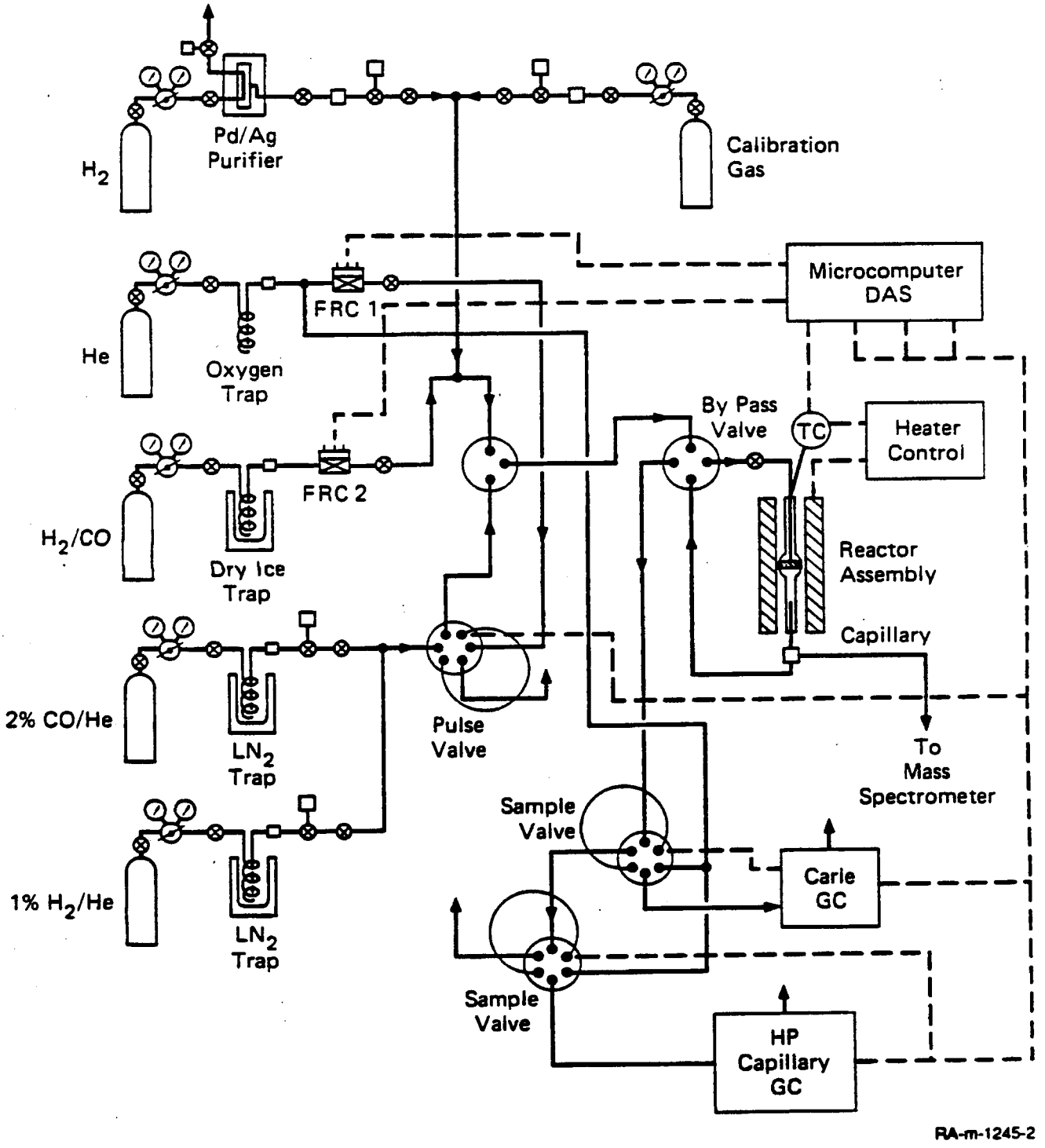

Figure I-8. Catalyst characterization and testing apparatus.

ratio of the rate of formation of methane relative to the overall hydrocarbon reaction rate for C_1 through C_{10} products (on a carbon-atom basis).

At 573 K using 2/1 H_2/CO synthesis gas, the ruthenium catalysts have very high selectivity for methane. The organometallic derived catalysts were more active than the conventional Ru catalyst. The activity at 523 K and 1/1 H_2/CO is summarized in Table I-6.

Slurry-Phase Reactor. The FTS activity and selectivity in the slurry phase were examined for four catalysts: the allyl-derived Ru monomer on a molecular sieve support, the aluminum-hydridocarbonyl-derived Ru_4 cluster catalyst on an Na-Y zeolite support, a conventional Ru catalyst on alumina, and the fused iron standard catalyst (Table I-7). The reactor set-up was similar to that used by Huff and Satterfield.[67] In a 300-mL slurry reactor, 2 g of powdered catalyst was used with 50 g of n-octocosane wax (n-$C_{28}H_{58}$, 99%, Alfa Chemical) with 1:1 $CO:H_2$ syngas at 60 atm and 483 K (10 K) for 48 h. The gas outlet was connected to a high temperature trap (100°C). The hydrocarbon distribution of the product gas up through C_4 was directly analyzed periodically by capillary GC with FID detection. Condensation in the sample lines precluded observation of hydrocarbon above butane.

The liquid product distribution was analyzed by FIMS after the synthesis run. We were unable to detect higher hydrocarbons from any of these slurry runs because of the high concentration of the n-octocosane. (Calibration of the FIMS technique using FTS wax provided by Professor Satterfield of MIT is described in Section II.[68])

Discussion

The organometallic derived catalysts showed activity similar to that observed for the conventional ruthenium catalyst in fixed-bed tests at 523 K as shown in Table I-6. The most active catalysts were the tetrameric ruthenium cluster on alumina and sodium Y-zeolite, followed by the monomeric ruthenium on 5-Å molecular sieves. However, under these conditions all the catalysts gave distributions that were not

Table 1-6

FTS PERFORMANCE OF RUTHENIUM CLUSTER AND CONVENTIONAL RUTHENIUM CATALYSTS

Catalyst	Ru/Na-Y Zeolite 0.31 wt% Ru	Ru_4/Na-Y Zeolite 0.61 wt% Ru	Ru_6/Na-Y Zeolite 0.20 wt% Ru	Ru/5A Molecular Sieve 0.37 wt% Ru	Ru_4/5A Molecular Sieve 0.49 wt% Ru	Ru_6/5A Molecular Sieve 0.19 wt% Ru	Ru/Al_2O_3 0.35 wt% Ru	Ru_4/Al_2O_3 0.61 wt% Ru	Ru_6/Al_2O_3 1.2 wt% Ru	Conventional Ru/Al_2O_3 0.50 wt% Ru
Temperature (K)	523	523	523	523	523	523	523	523	523	523
Pressure (MPa)	0.01	0.01	0.01	0.1	0.1	0.1	0.1	0.1	0.1	0.1
H_2/CO ratio	1	1	1	1	1	1	1	1	1	1
Run duration (h)	24	16	20	24	24	24	24	19	22	24
Product rate[a] (nmol/s/g cat)										
CO_2	2.31	2.96	3.68	3.16	2.25	2.73	1.09	2.73	4.03	2.1
C_1	3.54	7.63	0.78	12.19	6.68	4.41	2.82	12.67	9.23	6.32
C_2	0.47	0.994	0.158	0.81	0.81	0.87	0.51	1.19	0.87	0.65
C_3	0.55	1.044	0.27	0.57	0.7	0.56	0.594	1.05	0.76	0.684
C_4	0.22	0.392	0.104	0.155	0.24	0.19	0.198	0.33	0.29	0.23
C_5	0.77	0.138	0.012	0.029	0.091	0.053	0.058	0.12	0.114	0.081
C_6	0.75	0.066			0.047	0.028	0.022	0.068	0.073	0.04
C_7	0.48	0.033			0.032	0.0088	0.007	0.031	0.039	0.019
C_8	0.26	0.017			0.016	0.004	0.005	0.015	0.021	0.008
C_9					0.0091			0.0053	0.0073	0.004
C_{10}					0.0074			0.0043	0.0058	
TOTAL	8.39	15.77	2.382	16.29	12.605	9.117	6.93	20.958	15.983	11.51
Chain Growth Factor[b]	0.57	0.48		0.23	0.46	0.39	0.37	0.45	0.43	0.47
Olefin to Paraffin Ratio[c]	2.02	1.2		1.4	0.77	1.3	3.2	1.1	1.1	1.3
Methane Selectivity[d]	45	52	36	77	56	52	44	61	63	58

[a] GHSV = 600 h^{-1}; Product rate for each carbon number includes n-paraffins and α- and β-olefins; total product rate is on a carbon-atom basis.

[b] Average chain growth parameter (α) for C_{3+} hydrocarbons.

[c] Average olefin to paraffin ratio for C_2 to C_6 hydrocarbons.

[d] C_1 rate/(total rate) x 100%.

Table 1-7

RESULTS OF SLURRY REACTOR FTS EXPERIMENTS

Catalyst	Clean Fused Iron	Ru_4/Na-Y Zeolite 0.61 wt% Ru	Ru/5A Molecular 0.37 wt% Ru	Conventional Ru/Al_2O_3 0.50 wt% Ru
Temperature (K)	493	493	493	493
Pressure (MPa)	6.9	6.9	6.9	6.9
H_2/CO ratio	1	1	1	1
Run duration (h)	48	48	48	48
CO_2	90.932	15.932	0.262	1.094
C_1	11.629	9.031	0.536	0.24
C_2	6.211	2.215	0.106	0.0063
C_3	5.91	1.349	0.041	0.022
C_4	3.23	0.568	0.0176	0.0187

[a]GHSV = 600 h^{-1}; Product rate for each carbon number includes n-paraffins and α- and β-olefins; total product rate is on a carbon-atom basis.

[b]Average chain growth parameter (α) for C_{3+} hydrocarbons.

[c]Average olefin to paraffin ratio for C_2 to C_6 hydrocarbons.

[d]C_1 rate/(total rate) x 100%.

significantly different from that of ASF. The methane selectivity was in the range of 36 to 77 mol%. To more closely approach the condition of "living polymers," we had to increase the pressure. This was done in a slurry reactor at approximately 60 atm. We compared a clean fused iron and a conventional ruthenium catalyst to the tetraruthenium on Y-zeolite and the mononuclear ruthenium on 5-Å molecular sieves (Table I-7). Of the four catalysts tested, the iron and the Ru_4/Na-Y-zeolite showed very high activity, whereas the mononuclear Ru and the conventional Ru showed very low activity. Only the conventional Ru showed high chain growth probabilities and low methane selectivities that would be expected for slurry reactions. In no case could we observe any wax products in the slurry by FIMS after 48 h.

Unfortunately, the results of the slurry reactor experiments neither deny nor verify the hypothesis that the cluster catalysts can produce a narrowed FTS product distribution. The FIMS analysis of slurry liquid samples at the end of the experiments was not adequate even to resolve the high-molecular-weight product distribution for the conventional catalysts, and we could not have expected to measure the product distribution in the C_{12+} range for the cluster catalysts. Additional slurry runs with much longer reaction time (at least 200 h) must be performed in future work to test the cluster hypothesis. However, the low chain growth factor and the presence of light alkanes in the gaseous product indicates that we may not have reached the state of "living polymers."

References

1. M. E. Dry and J. C. Hoogendoorn, Catal. Rev. 23, 265 (1981).

2. M. E. Dry, "The Fischer-Tropsch Synthesis," in Catalysis Science and Technology, J. B. Anderson and M. Boudart, Eds. (Springer-Verlag, 1981), p. 159.

3. D. L. King, J. A. Cusumano, and R. L. Garten, Catal. Rev. 23, 203 (1981).

4. A. T. Bell, Catal. Rev. 23, 203 (1981).

5. C. K. Rofer-DePoorter, Chem. Rev. 31, 447 (1981).

6. P. Biloen and W.M.H. Sachtler, Adv. Catal. 30, 165 (1981).

7. H. H. Starch, N. Golumbic, and R. B. Anderson, The Fischer-Tropsch Synthesis (Wiley, 1951).

8. G. Henrici-Olive and S. Olive, J. Mol. Catal. 24, 7 (1984).

9. G. Henrici-Olive and S. Olive, The Chemistry of the Catalyzed Hydrogenation of Carbon Monoxide (Springer-Verlag, 1984).

10. V. A. Zakharov, G. D. Bukatov, and Y. I. Yermakov, Adv. Polym. Sci. 51, 63 (1983).

11. V. Zucchini and G. Cecchin, Adv. Polym. Sci. 51, 103 (1983).

12. K. W. McLaughlin and C.A.J. Hoeue, Polym. Prep. 27, 257 (1986).

13. G. Henrici-Olive and S. Olive, Adv. Polym. Sci. 15, 1 (1974).

14. Y. Doi, S. Ueki, and T. Keii, Macromolecules 12, 814 (1979).

15. M. Roper, "Fischer-Tropsch Synthesis," in Catalysis in C_1 Chemistry, W. Keim, Ed. (D. Reidel, 1983), p. 41.

16. V. H. Pichler, B. Firnhaber, D. Kioussis, and N. Dowallace, Makromol. Chem. 70, 12 (1964).

17. V. H. Kolbel, W.H.E. Muller, and H. Hammer, Makromol. Chem. 70, 1 (1964).

18. R. J. Madon, J. Catal. 57, 183 (1979).

19. D. L. King, J. Catal. 51, 386 (1978).

20. C. S. Kellner and A. T. Bell, J. Catal. 70, 418 (1981).

21. R. A. Stowe and C. B. Murchison, Hydrocarbon Processing, p. 95 (June 1984).

22. F. King, E. Shutt, and A. I. Thomson, Platinum Met. Rev. 29, 146 (1985).

23. M. Audier, J. Klinowski, and R. E. Benfield, J. Chem. Soc. Chem. Commun., p. 626 (1984).

24. K. J. Smith and R. C. Everson, J. Catal. 99, 349 (1986).

25. Z.-Z. Lin, T. Okuhara, and M. Misono, Chem. Lett. p. 913 (1986).

26. T. Okuhara, T. Enomoto, H. Tamura, and M. Misono, Chem. Lett., p. 1491 (1984).

27. T. Enomoto, K. Kaba, T. Okuhara, and M. Misono, Bull. Chem. Soc. Jpn. 60, 1237 (1987).

28. Y. Doi, H. Miyake, and K. Soga, J. Chem. Soc. Chem. Commun. p. 347 (1987).

29. T. Mori, A. Miyamoto, N. Takahashi, M. Fukagaya, H. Niizuma, T. Hattori, and Y. Murakami, J. Chem. Soc. Chem. Commun., p. 678 (1984).

30. T. Mori, S. Taniguchi, Y. Mori, T. Hattori, and Y. Murakami, J. Chem. Soc. Chem. Commun. p. 1401 (1987).

31. N. Takahashi, T. Mori, A. Miyamoto, T. Hattori, and Y. Murakami, Appl. Catal. 38, 61 (1988).

32. N. Takahashi, T. Mori, A. Miyamoto, T. Hattori, and Y. Murakami, Appl. Catal. 38, 301 (1988).

33. N. Takahashi, T. Mori, A. Furuta, S. Komai, A. Miyamoto, T. Hattori, and Y. Murakami, J. Catal. 110, 410 (1988).

34. T. Tatsumi, Y. G. Shul. T. Sugiuna, and H. Tominaga, Appl. Catal. 21, 119 (1986).

35. Y. G. Shul, T. Sugiura, T. Tatsumi, and H. Tominaga, Appl. Catal. 24, 131 (1986).

36. Y. G. Shul, Y. Arai, T. Tatsumi, and H. Tominaga, Bull. Chem. Soc. Jpn. 60, 2335 (1987).

37. H. H. Nijs, P. A. Jacobs, and J. B. Uytterhoeven, J. Chem. Soc. Chem. Commun., p. 180 (1979).

38. D. Balliuet-Tkatchenko, G. Coudurier, H. Mozzanega, and I. Tkatchenko, Fund. Res. Homogeneous Catal. 3, 257 (1979).

39. D. Fraenkel and B. C. Gates, J. Am. Chem. Soc. 102, 2478 (1980).

40. H. Nijs, P. A. Jacobs, and J. B. Uytterhoeven, J. Chem. Soc. Chem. Commun., p. 1095 (1979).

41. H. H. Nijs and P. A. Jacobs, J. Catal. 65, 328 (1980).

42. D. Balliuet-Tkatchenko, N. D. Chau, H. Mozzanega, M. C. Roux, and I. Tkatchenko, ACS Symp. Ser. 152, 187 (1981).

43. F. Hugues, P. Bussiere, J. M. Basset, D. Commercoc, Y. Chaurin, L. Bonneviot, and D. Olivier, Proc. 7th Int. Congr. Catal., Tokyo, 1980, T. Seiyama and K. Tanabe, Eds. (Elsevier, 1981), p. 418.

44. Y. W. Chen, H. T. Wang, and J. G. Goodwin, Jr., J. Cataly. 85, 499 (1984).

45. R. K. Ungan and M. C. Baird, J. Chem. Soc. Chem. Commun. p. 643 (1986).

46. T.-A. Lin, L. H. Schwartz, and J. B. Butt, J. Catal. 97, 177 (1986).

47. J. B. Butt, J.-A. Lin, and L. H. Schwartz, J. Catal. 97, 261 (1986).

48. D.-K. Lee and S.-K. Ihm, J. Catal. 106, 386 (1987).

49. T. Bein, G. Schmiester, and P. A. Jacobs, J. Phys. Chem. 90, 4851 (1986).

50. P. A. Jacobs and D. Van Wouwe, J. Mol. Catal. 17, 145 (1982).

51. K. McLaughlin, Dow Chemical, private communication.

52. R. A. Dictor and A. T. Bell, Ind. Eng. Chem. Process Des. Dev. 22, 678 (1983).

53. E. Peacock-Lopez and K. Kindenberg, J. Phys. Chem. 88, 2270 (1984).

54. I. R. Leith, J. Catal. 91, 283 (1985).

55. T. Fukushima, K. Fujimoto, and H. Tominaga, Appl. Catal. 14, 95 (1985).

56. K. Fujimoto, T. Nobusawa, T. Fukushima, and H. Tominaga, Bull. Chem. Soc. Jpn. 58, 3164 (1985).

57. K. Fujimoto, H. Saima, and H. Tominaga, J. Catal. 94, 16 (1985).

58. L. Fu and C. H. Bartholomew, J. Catal. 92, 376 (1985).

59. C. D. Chang, J. N. Miale, and R. F. Socha, J. Catal. 90, 84 (1985).

60. Y. Iwasawa and N. Itō, J. Catal. 96, 613 (1985).

61. M. Logan, A. Gellman, and G. A. Somorjai, J. Catal. 94, 60 (1985).

62. Y. I. Yermakov, B. N. Kuznetsov, and V. A. Zakharov, Catalysis by Supported Complexes (Elsevier, 1981).

63. A. A. Bhattacharyya, C. C. Nagel, and S. G. Shore, Organometallics 2, 1187 (1983).

64. B.F.G. Johnson, J. Lewis, P. R. Raithby, and G. Suss, J. Chem. Soc. Dalton Trans., p. 1356 (1978).

65. G. Sbrana, G. Braca, F. Piacenti, and P. Pino, J. Organomet. Chem. 13, 240 (1968).

66. E. W. Abel and S. Moorhouse, J. Chem. Soc. Dalton Trans., p. 1706 (1973).

67. G. A. Huff, Jr. and C. N. Satterfield, Ind. Eng. Chem. Fundam. 21, 479 (1982).

68. H. G. Stenger, H. E. Johnson, and C. N. Satterfield, J. Catal. 86, 1477 (1984).